

1 **Transformed-Stationary EVA 2.0: A Generalized Framework for** 2 **Non-Stationary Multivariate Extremes Analysis**

3 Mohammad Hadi Bahmanpour¹, Alois Tilloy², Michalis Vousdoukas³, Ivan Federico⁴, Giovanni
4 Coppini⁴, Luc Feyen², Lorenzo Mentaschi^{1,4}

5 ¹ Department of Physics and Astronomy “Augusto Righi” (DIFA), University of Bologna, Bologna, Italy

6 ² European Commission, Joint Research Centre, Ispra, Italy

7 ³ Department of Marine Sciences, University of Aegean, University Hill, Mytilene, Greece

8 ⁴ CMCC Foundation - Euro-Mediterranean Center on Climate Change, Italy

9 *Corresponding to: Mohammad Hadi Bahmanpour (hadi.bahmanpour@unibo.it), Lorenzo Mentaschi*
10 *(lorenzo.mentaschi@unibo.it)*

11 **Abstract.** The increasing availability of extensive time series on natural hazards underscores the need for robust non-
12 stationary methods to analyze evolving extremes. Moreover, growing evidence suggests that jointly analyzing phenomena
13 traditionally treated as independent, such as storm surge and river discharge, is crucial for accurate hazard assessment. While
14 univariate non-stationary extreme value analysis (EVA) has seen substantial development in recent decades, a comprehensive
15 methodology for addressing non-stationarity in joint extremes—compound events involving simultaneous extremes in
16 multiple variables—is still lacking. To fill this gap, here we propose a general framework for the non-stationary analysis of
17 joint extremes that combines the Transformed-Stationary Extreme Value Analysis (tsEVA) approach with Copula theory.
18 This methodology implements sampling techniques to extract joint extremes, applies tsEVA to estimate non-stationary
19 marginal distributions using GEV or GPD distributions, and utilizes time-dependent copulas to model evolving inter-variable
20 dependencies. The approach’s versatility is demonstrated through case studies analyzing historical time series of significant
21 wave height, river discharge, temperature, and drought, uncovering dynamic dependency patterns over time. To support
22 broader adoption, we provide an open-source MATLAB toolbox that implements the methodology, complete with examples,
23 available on GitHub.

1. Introduction

Extreme value analysis (EVA), or frequency analysis of extreme events, is crucial for understanding the likelihood of catastrophic events. By quantifying the probabilities of such occurrences, EVA informs design approaches and supports the development of better management strategies. Traditionally, EVA assumes stationarity, meaning that the statistical properties of the data, such as mean and variance, remain constant over time (Coles, 2001). However, many long-term datasets reveal varying degrees of non-stationarity, often due to anthropogenic influences and natural climate variability. Ignoring non-stationarity can lead to inaccurate estimates of probabilities and return levels, underscoring the importance of accounting for time-dependent changes in the frequency and intensity of extreme events (Cheng, et al., 2014).

In a univariate framework, non-stationarity refers to temporal changes in the frequency or magnitude of a single random variable. Univariate non-stationary EVA is a relatively well-explored topic (e.g., Cannon, 2010; Parey, et al., 2010). A common approach to address non-stationarity involves defining a parametric form for its variation, potentially as a function of covariates, and using optimization methods, such as the Maximum Likelihood Estimator (MLE), to determine the optimal parameters that capture both the non-stationary behavior and the distribution of extreme values. Other methods focus on stationarizing the input series and performing EVA on this stationarized data (Parey et al., 2010; Parey et al., 2013; Mentaschi et al., 2016; Acero et al., 2017; Parey et al., 2019). Mentaschi et al. (2016) proposed an alternative approach to univariate non-stationary EVA that decouples the detection of non-stationarity from the fit of the Extreme Value Distribution (EVD). Known as transformed-stationary EVA (tsEVA), this method transforms a non-stationary signal into a stationary one, avoiding the need for predefined parametric forms for non-stationarity. Unlike traditional methods, which parameterize time-dependent changes and optimize them alongside the EVD parameters, tsEVA focuses on ensuring that the transformed signal adheres to the principles of asymptotic extreme value theory. While mathematically equivalent to traditional approaches, tsEVA offers key advantages: (a) it does not rely on assuming specific parametric forms for non-stationarity and (b) it provides intermediate diagnostics to verify the effectiveness of the transformation. This well-established methodology has been widely adopted in various studies for univariate non-stationary EVA (e.g., Mentaschi et al., 2017; Dosio et al., 2018; Naumann et al. 2021; Vousdoukas et al., 2018; Dottori et al., 2023).

From a risk assessment perspective, studies (e.g. Zscheischler et al. 2018, 2020) have highlighted that univariate approaches can misrepresent the probability of joint extreme events, particularly in risk management and infrastructure design. Multivariate extreme value analysis (EVA) provides a more robust framework for accurately quantifying risk in such contexts (Tilloy, et al., 2020). Its applications span a wide range of hazards, including drought-heatwave events (e.g. Manning et al. 2019), compound hydrological events (e.g. Bevaqua et al. 2017; Jiang et al. 2022), and coastal hazard (e.g. Bevaqua et al. 2019).

Similar to the univariate case, multivariate extreme value analysis (EVA) for datasets with long temporal coverage must account for the non-stationarity of the underlying signals. Several studies have investigated non-stationary joint distributions, though these efforts often focus on specific applications rather than development of general methodologies. For example, Bender et al. (2014) applied a non-stationary statistical model to analyze the time-varying joint distribution of flood peak and volume for the Rhine River. Wahl et al. (2015) analyzed the joint occurrence of storm surge and precipitation for major US coastal cities and demonstrated that compound flooding events have increased significantly over the past century, with higher risk along the Atlantic and Gulf coasts. Jiang et al. (2015) examined how reservoir construction influenced joint return periods of low river flow downstream, incorporating

71 non-stationarity in both marginal distributions and dependence structures using temporal variation and
72 covariates. Similarly, Sarhadi et al. (2016) assessed non-stationary drought characteristics, including
73 severity and duration, by combining historical and projected Standardized Precipitation Index (SPI)
74 data under various climate scenarios. Li et al. (2019) studied spatial variations in extreme precipitation,
75 modeling non-stationarity in margins and dependencies through a linear regression applied to a 30-year
76 moving time window.
77 Despite these efforts, such applications are often tailored to specific problems and lack generalizability.
78 While univariate non-stationary EVA is relatively well-studied, multivariate non-stationary EVA
79 remains an underexplored field with no widely accepted standard approach. To address this gap, here
80 we extended the tsEVA methodology to develop a versatile method for the multivariate analysis of
81 non-stationary extremes, grounded in copula theory (Sklar, 1959, 1973). This enhanced framework
82 provides a generalizable solution for capturing the dependence structures and time-varying
83 characteristics of extreme events across multiple variables. The capabilities of the resulting open-
84 source MATLAB toolbox, tsEVA 2.0, are demonstrated in this study through a series of applications
85 that showcase its utility in different scenarios. These examples highlight the potential of tsEVA 2.0 to
86 advance the understanding and modeling of multivariate non-stationary extremes in a range of
87 scientific and engineering contexts.

88 2. Data and Methods

89 Non-stationary copula

91 The term 'copula', introduced by Sklar's theorem (1959), refers to a mathematical tool that describes the
92 dependency between different univariate distributions, known as marginals in this context. Given a set
93 of random variables (Y_1, \dots, Y_m) with marginal distributions F_1, \dots, F_m and joint distribution function
94 $H \in \mathcal{H}(y_1, \dots, y_m)$, the copula C is a function defined in the probability space such that:

$$95 H_{Y_1, \dots, Y_m}(y_1, \dots, y_m) = C(F_{Y_1}(y_1), \dots, F_{Y_m}(y_m)) \quad (1)$$

96 Equation (1) illustrates why copulas are widely used in higher-dimensional statistics, as they enable
97 separate modeling of the marginals and their dependency structure, simplifying the construction of joint
98 distributions. For a more detailed description of the copula theory, the reader is referred to Joe (1997)
99 and Nelsen (2006). In this study we considered three well-established types of copulas (Table 1):

- 100 1. **Gaussian copula.** In this copula, the joint probability density function exhibits symmetry around a
101 central point, with the contours of constant density forming ellipsoids in the multivariate space. The
102 Gaussian copula models situations where the dependency structure between two variables remains
103 constant across the entire distribution and does not exhibit tail dependence.
- 104 2. **Gumbel copula.** This is an Archimedean copula, i.e. it models the dependencies among variables using
105 a function of the marginal probability, called "generation function", able to capture non-linear
106 dependencies. In particular, the Gumbel copula can adequately reproduce conditions when the
107 dependency among variables is stronger for the upper tails. For higher-dimensional cases (trivariate and
108 above), we use a C-vine construction, which builds the multivariate dependence from pairwise Gumbel
109 copulas in a hierarchical tree structure.
- 110 3. **Frank copula.** This is an Archimedean copula that suits situations that are tail-independent in both tails,
111 meaning that as values approach extreme highs or lows, the dependence between them weakens.
112

116 Table 1: list of copula functions implemented in tsEVA 2.0. In the table, the symbol $\phi()$ represents the standard normal distribution. For
 117 Archimedean copulas (e.g., Gumbel and Frank) $\gamma_\theta(\chi)$ denotes the generator function used in constructing the copula
 118 $c_{(u,v|\theta)} = \gamma_\theta^{-1}[\gamma_\theta(u) + \gamma_\theta(v)]$.
 119

Copula	$c(u,v \theta)$	$\gamma_\theta(\chi)$	Parameter range
Gaussian	$\int_{-\infty}^{\phi^{-1}(u)} \int_{-\infty}^{\phi^{-1}(v)} \frac{1}{2\pi\sqrt{1-\theta^2}} \exp\left(\frac{2\theta xy - x^2 - y^2}{2(1-\theta^2)}\right) dx dy$	-	$\theta \in [-1, 1]$
Gumbel	$\exp\left\{-\left[(-\ln u)^\theta + (-\ln v)^\theta\right]^{1/\theta}\right\}$	$(-\ln \chi)^\theta$	$\theta \in [1, \infty)$
Frank	$-\frac{1}{\theta} \ln\left(1 + \frac{(e^{-\theta u} - 1)(e^{-\theta v} - 1)}{e^{-\theta} - 1}\right)$	$-\ln \frac{e^{-\theta \chi} - 1}{e^{-\theta} - 1}$	$\theta \in \mathbb{R} \setminus 0$

120
 121 To describe the time evolution of the copula, we evaluated a time-varying coupling parameter θ_t on a
 122 moving window, similar to what proposed by Li, et al., (2019). The duration of series is covered by N
 123 time windows where:

$$124 \quad N = \left\lfloor \frac{T-w}{\Delta t} \right\rfloor + 1 \quad (2)$$

125 Where T is the length of the series (in years), w is the window length (in years), $\Delta t = 1$ is the window
 126 shift (sliding by 1 year), and N is the number of moving windows. The symbol $\lfloor \cdot \rfloor$ ensures a floor
 127 operation.

128
 129 Non-stationary marginals

130
 131 The treatment of the marginals (i.e., the distributions of the univariates, F_1, \dots, F_m in Eq. (1)), was
 132 performed in accordance with the univariate theory of extremes. There are two popular approaches that
 133 are used to model extremes of a series. The Fisher-Tippett-Gnedenko theorem establishes the
 134 Generalized Extreme Value (GEV) distribution as the appropriate distribution for statistically
 135 homogeneous block maxima, such as annual maxima. The cumulative GEV distribution is defined as:
 136

$$137 \quad GEV_X(x; \varepsilon, \mu, \sigma) = \exp\left\{-\left[1 + \varepsilon \left(\frac{x-\mu}{\sigma}\right)\right]^{-1/\varepsilon}\right\}, \quad (3)$$

138
 139 where ε, μ , and σ are the shape, location and scale parameters, that need to be found out through a
 140 fitting process. On the other hand, the Generalized Pareto Distribution (GPD) is the general form of the
 141 distribution of the Peaks Over Threshold (POT) according to the Pickands–Balkema–De Haan theorem.
 142 The cumulative GPD is defined as

$$144 \quad GPD_{X-u}(\tilde{x}; \varepsilon, \tilde{\sigma}) = 1 - \left(1 + \frac{\varepsilon \tilde{x}}{\tilde{\sigma}}\right)^{-1/\varepsilon}, \quad (4)$$

145
 146 where $\tilde{x} = x - u$ is the series of excess values relative to the selected threshold value (u), and ε and $\tilde{\sigma}$
 147 are the shape and scale parameters respectively (Coles, 2001).

148 To address non-stationarity in the marginal distributions, we adopted the approach proposed by
 149 Mentaschi et al. (2016), which demonstrates that a transformation formally equivalent to local
 150 normalization allows for a generalized representation of non-stationary extreme value distributions
 151 while maintaining a constant shape parameter. Specifically, the transformation f is defined as:

$$153 \quad y(t) \xrightarrow{f(y,t)} x(t) \quad \text{where} \quad f(y,t) = \frac{y(t) - T_y(t)}{c_y(t)} \quad (5)$$

154

155 where $y(t)$ is the non-stationary series, $x(t)$ is the assumed stationary series, $T_y(t)$ and $C_y(t)$ are
 156 generic terms representing the long-term variation in the mean and amplitude of $y(t)$, respectively. A
 157 back-transformation from the stationary domain x to the non-stationary one y leads to a formulation of
 158 parameters of time-varying extreme values distribution. In particular, for the GEV one obtains:

$$159 \begin{cases} \varepsilon_y = \varepsilon_x \\ \sigma_y(t) = C_y(t) \cdot \sigma_x \\ \mu_y(t) = C_y(t) \cdot \mu_x + T_y(t) \end{cases}, \quad (6)$$

160
 161 and for the GPD:

$$162 \begin{cases} \varepsilon_y = \varepsilon_x \\ \tilde{\sigma}_y(t) = C_y(t) \cdot \tilde{\sigma}_x \\ u_y(t) = C_y(t) \cdot u_x + T_y(t) \end{cases}. \quad (7)$$

164
 165
 166 Joint sampling of the extremes

167
 168 There are several methods to sample joint extremes from multivariate data (e.g., Zheng et al., 2014).
 169 The simplest method used in tsEVA 2.0 applies a block-maxima technique, compatible with GEV-
 170 distributed marginals, focusing on the coupling of annual maxima from each variable. A key limitation
 171 of this method, inherent to the GEV distribution, is that not all extremes are annual maxima, nor are all
 172 annual maxima truly extreme events. Additionally, this approach may link events far apart in time
 173 while missing those that occur close together but fall across block boundaries. Despite these
 174 limitations, its simplicity makes it effective for studying dependencies among relatively slow, seasonal
 175 phenomena, such as drought and heat waves.

176 A more advanced approach involves non-stationary joint Peaks Over Threshold (POT) sampling. This
 177 method first applies the transformation in Eq. (5) to convert each non-stationary signal $y(t)$ to a
 178 stationary series $x(t)$. POT sampling is then conducted on each stationarized series $x(t)$, selecting
 179 multivariate peaks within a defined maximum time interval $\Delta t_{multivariate}$. A challenge with this
 180 approach is the potential for multiple combinations of univariate peaks within the interval
 181 $\Delta t_{multivariate}$. In tsEVA 2.0, this issue is addressed by prioritizing joint peaks with the largest mean
 182 values (average of univariate peak values), iteratively removing all other peak combinations.

183
 184 Goodness-of-fit

185
 186 To evaluate the goodness-of-fit (GOF) of the copula model, a multi-parameter approach was employed
 187 by analyzing a set of statistics that quantify the similarity between the fitted distribution and the
 188 empirical data. Specifically, the following statistics were considered:

- 189 • Cramér-von Mises statistic. Its general definition is:

$$S_n = \int [C_n(u) - C_\theta(u)]^2 du, \quad (8)$$

190 where C_n is the empirical distribution, C_θ is the theoretical fit, u is defined in the domain of the
 191 distributions. The statistic S_n serves as a proxy for the distance between the empirical and
 192 theoretical distributions in probability space. In this study, we applied the rank-based version of the
 193 Cramér-von Mises statistic, where the ranks of C_n and C_θ are compared using Monte Carlo

194 simulations. For non-stationary distributions, S_n is estimated separately over different time
 195 windows, and the results are averaged, to provide the mean Cramér-von Mises statistic \overline{S}_n .

- 196
- 197 • For each bivariate sub-distribution, the goodness-of-fit was evaluated by comparing the correlation
 198 structure of the fitted copula to that of the original data. Specifically, the differences in Spearman's
 199 rank correlation coefficient ($\Delta\rho_{Spearman}$) and Kendall's tau ($\Delta\tau_{Kendall}$) were computed between a
 200 Monte Carlo simulation of the fitted copula distribution and the empirical values derived from the
 201 original sample. This provides a measure of how well the fitted model captures the dependency
 202 structure of the data. For multivariate non-stationary copulas, this analysis was extended by
 203 computing the average differences $\Delta\rho_{Spearman}$ and $\Delta\tau_{Kendall}$ over all the bivariate sub-distributions
 204 and the considered time windows. The metrics are defined as:

$$\overline{\Delta\rho_{Spearman}} = \frac{1}{N \cdot P} \sum_{t=1}^N \sum_{1 \leq i < j \leq d} |\rho_{t,(i,j)} - \rho_{t,(i,j),MC}| \quad (9)$$

$$\overline{\Delta\tau_{Kendall}} = \frac{1}{N \cdot P} \sum_{t=1}^N \sum_{1 \leq i < j \leq d} |\tau_{t,(i,j)} - \tau_{t,(i,j),MC}| \quad (10)$$

205

206 where $\rho_{t,(i,j)}$ and $\rho_{t,(i,j),MC}$ are the Spearman correlation of variables i and j at time window t for
 207 the original and Monte-Carlo samples, $P = \frac{d \cdot (d-1)}{2}$ is the total number of bivariate pairs, d is the
 208 total number of variables, N is the total number of windows, $\tau_{t,(i,j)}$ and $\tau_{t,(i,j),MC}$ are the Kendall
 209 correlation of variables i and j at time window t for the original and Monte-Carlo samples, and
 210 $\overline{\Delta\rho_{Spearman}}$ and $\overline{\Delta\tau_{Kendall}}$ are the absolute difference in Spearman and Kendall correlation
 211 averaged across time windows and across bivariate pairs of variables.
 212
 213

214 Bivariate Return Periods

215

216 In the non-stationary context, there is not any standard definition of a return period, and different
 217 propositions have been made (Yan et al. 2017). Therefore, the interpretation of return periods requires
 218 careful definition, and different frameworks have been proposed (Parey et al. 2010; Yan et al. 2017). In
 219 Parey et al. (2010), univariate return levels are computed for the stationary transformed variable and
 220 then back-transformed to represent a specific target future climate period. The tsEVA framework
 221 adopts a similar transformation-based philosophy but with a different implementation and
 222 interpretation.

223 Multivariate return periods can be defined in several ways (Serinaldi, 2015; Salvadori et al., 2016). In
 224 tsEVA 2.0, we adopted the following two definitions:

- 225
- 226 (1) A definition that is more relevant in risk analysis and represent simultaneous exceedance of variables
 227 over their given thresholds (the AND return period) which for bivariate case, reads as:

$$T_{u_1, u_2}^{AND} = \frac{\mu}{1 - u_1 - u_2 + C(u_1, u_2)} \quad (11)$$

- 228
- 229 (2) A definition that is closest to the definition of cumulative multivariate distribution function (the OR
 230 return period) which for the bivariate case, reads as:
 231

$$T_{u_1, u_2}^{OR} = \frac{\mu}{1 - C(u_1, u_2)} \quad (12)$$

233

234 where μ is the average inter-arrival time, representing the mean time between peaks and $u_i = F_{x_i}(x_i)$
 235 represents continuous marginal distributions. The OR return period (T_{u_1, u_2}^{OR}) refers to the case where
 236 at least one of the x_i values is exceeded while the AND return period T_{u_1, u_2}^{AND} represent the case where
 237 both of the variables have exceeded x_i values. In bivariate analysis, joint probabilities associated with
 238 return periods form level curves (also known as isolines). Based on the above definition, we restricted
 239 the use of joint return periods to bivariate cases only. In the non-stationary context, return periods are
 240 conditional on the statistical properties (marginals and dependence) of each time window. The
 241 computation procedure is as follows: For each time window, we estimate (i) the time-varying marginal
 242 distributions from the back-transformed non-stationary GEV or GPD parameters, and (ii) the copula
 243 function $C(u, v)$ from the coupling parameter specific to that window. These are combined using the
 244 AND and OR definitions (Eq. (11) and Eq. (12)) to compute joint exceedance probabilities.

245

246 Detection of non-stationarity

247 The Mann-Kendall (MK) test is a nonparametric method used to detect trends in data over time. It
 248 compares pairs of data points to identify a consistent upward or downward trend. After calculating a
 249 test statistic, a p-value is obtained and compared to a chosen significance level (α) to determine
 250 whether the trend is statistically significant. A p-value below α indicates a significant trend, while a
 251 larger p-value suggests the trend is not statistically significant. A commonly used value for α is 0.05,
 252 but it can be adjusted depending on the context and requirements of the analysis.

253 We used MK to assess non-stationarity of the univariate marginals by applying the test on the annual
 254 percentile series. To see the effectiveness of transformation, the test was applied on both stationary and
 255 non-stationary series (i.e., before and after application of transformation). This method was applied as a
 256 shortcut to other sophisticated tests for stationarity that rely on bootstrapping (e.g., Parey, et al., 2013).
 257 To assess the non-stationarity of the joint distribution, we applied the modified Mann-Kendall test
 258 (Hamed 2008; Hamed and Rao 1998; Yue and Wang 2004), which explicitly accounts for
 259 autocorrelation arising from the 1-year sliding window used to compute the temporal evolution of the
 260 coupling parameter. By considering this autocorrelation, the test provides a more accurate assessment
 261 of statistical significance, avoiding the overestimation of trend significance that can occur with
 262 overlapping windows.

263

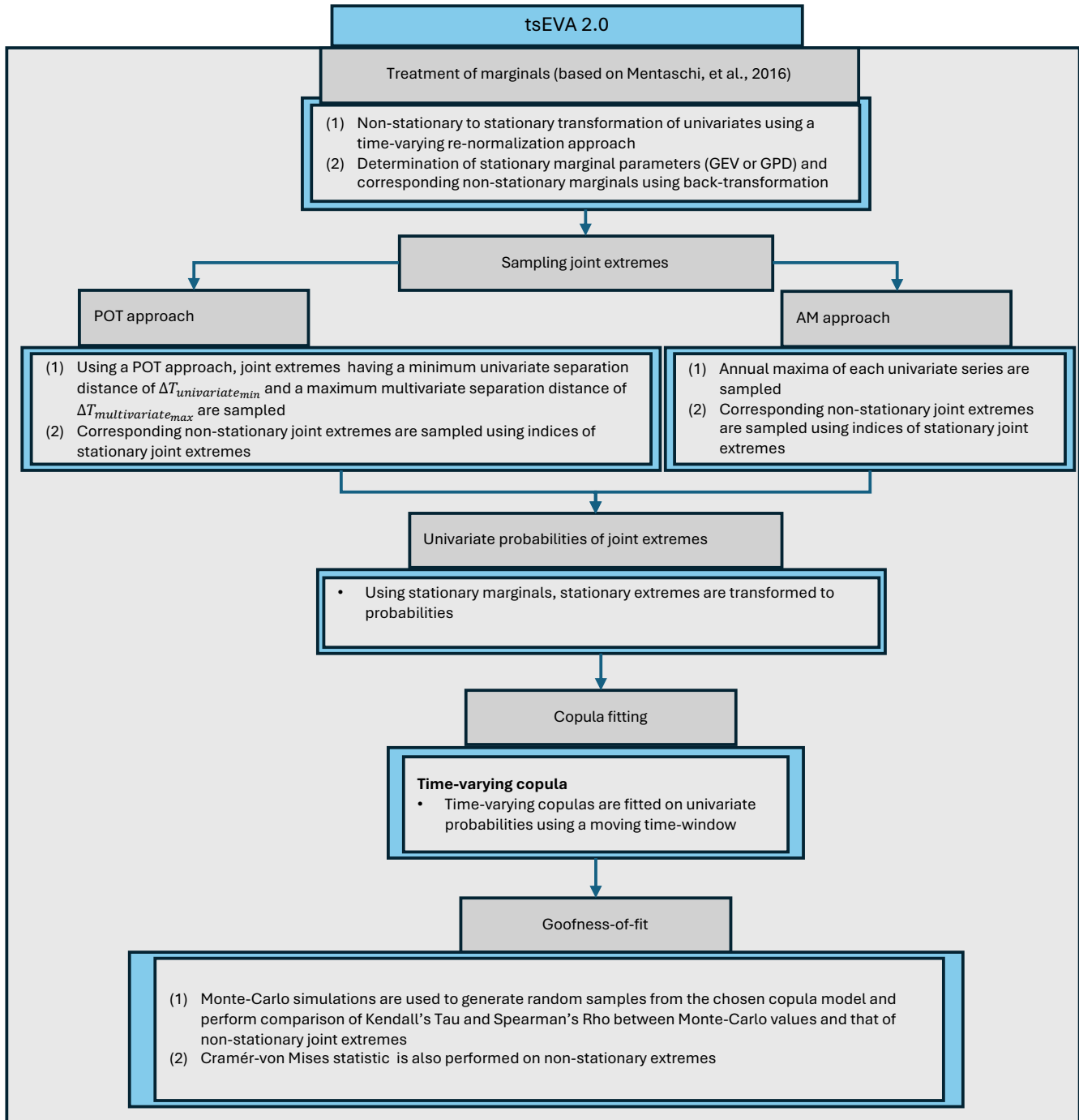
264 Assembling the Pieces: the tsEVA 2.0 toolbox

265

266 The methodologies outlined above are integrated into a MATLAB toolbox tsEVA 2.0, an extension of
 267 the original tsEVA by Mentaschi, et al., 2016, providing a versatile framework for multivariate analysis
 268 of non-stationary extremes across various applications. The toolbox features two primary functions:
 269 one employing non-stationary multivariate POT sampling with GPD and the other utilizing multivariate
 270 block-maxima sampling with GEV (Fig. 1).

271 In both approaches, the analysis begins by applying tsEVA's method to transform each univariate time
 272 series from non-stationary to stationary. The extreme value distribution (either GPD or GEV) is then
 273 fitted to the stationary series, and the resulting distributions are back-transformed into the time-varying
 274 domain to represent the non-stationary marginals. Joint extremes are subsequently sampled and
 275 mapped into probability space using the stationary marginals. A copula is then fitted to this transformed
 276 dataset, which can either be stationary (assuming constant dependency over time) or non-stationary

277 (accounting for time-varying dependency). To ensure the appropriateness of each copula model in
 278 representing the joint distribution of non-stationary extremes, we developed a dedicated goodness-of-fit
 279 routine. A flowchart of tsEVA 2.0 is presented in Fig. 1.
 280



281
 282 *Figure 1: Flowchart of tsEVA 2.0*

283
 284
 285 Case studies
 286

287 To demonstrate the applications of the general method developed for analyzing non-stationary joint
288 extremes, the methodology was applied to three case studies, each selected to highlight specific
289 features of the new methodology. All the data in the following examples were obtained from model
290 results. Possible biases in the model data can also find its way into quantification of return periods.
291 Nonetheless, these model outputs provided a good basis upon which the general methodology
292 developed in this paper could be substantiated. For the wave dataset used in the first and second case
293 study, we used a bias-corrected version of the results reported in Mentaschi, et al., 2023. The bias
294 correction was based on Quantile mapping, and we focused on values above 50th percentile. The bias-
295 correction was based on comparison with satellite measurements.

296

297 **1. Joint extremes of river discharge and wave height:**

298 This case study explored the evolving relationship between river discharge and significant wave height
299 (SWH) near the coast over time. The focus was on the mouth of the La Liane River in France, a fast-
300 responding river influenced by precipitation. Wave data comprised 3-hourly SWH records from a high-
301 resolution global wave model (Mentaschi et al., 2023) with nearshore resolutions of 2–4 km, covering
302 the period 1950–2020. River discharge data was obtained from the HERA hydrological reanalysis
303 (Tilloy et al. 2025). The dataset, generated with the OS LISFLOOD model (Burek et al. 2013),
304 provides high resolution (approx. 1.5 km) simulation of river discharge for every river with an
305 upstream area $>100\text{km}^2$ across Europe.). The data comes at six-hourly records over the same time
306 frame. Although residual model biases contribute to uncertainty in return level estimation, the use of
307 model data for coastal hazard mapping is widely established practice, as models provide complete
308 spatiotemporal coverage that cannot be achieved through sparse observational networks. The wave
309 dataset employed in this study (Mentaschi et al., 2023) was post-processed to reduce biases through
310 quantile mapping against satellite observations. Likewise, the river discharge dataset (Tilloy et al.
311 2025) was evaluated using 2448 river gauging stations to assess model skill.

312 The analysis used the Generalized Pareto Distribution (GPD) for univariate margins and a time-varying
313 Gumbel copula to model dependence. Univariate peaks were selected with a minimum separation of 30
314 days. In this case study, joint extremes were defined as events in which the peak of river discharge
315 occurred within a maximum time lag of 45 days after the peak of wave height. The choice of a 45-day
316 maximum allowable lag among bivariate peaks reflects the time-lag among univariate peaks (30 days)
317 and the impact-based temporal compounding perspective (Zscheischler et al., 2020): when an extreme
318 sea level event compromises coastal system capacity, a subsequent extreme river discharge within 45
319 days can produce amplified impacts even without direct hydrodynamic interaction. Following
320 sampling, the average temporal separation among bivariate peaks was approximately 15 days. Non-
321 stationarity of the joint distribution was assessed within a 40-year moving window, with thresholds set
322 at the 95th percentile for river discharge and the 99th percentile for wave height. On average, each 40-
323 year window contains 66 joint extremes, which provides adequate sample sizes for stable copula
324 parameter estimation.

325

326 **2. Spatial correlation of extreme wave heights across three locations:**

327 The second case study evaluated the spatial relationship of SWH across three locations scattered
328 around the Marshall Islands, using the same source for wave dataset as the first case study. This
329 trivariate analysis highlighted spatial dependencies, employing a non-stationary Gumbel copula with
330 non-stationary margins, modeled with GPD. Each variable was sampled at the 99th percentile, with
331 univariate peaks spaced a minimum of 12 hours apart and a maximum allowable distance of 12 hours
332 for multivariate peaks. A 40-year time window was used for the joint distribution. Each time window
333 contained 76 joint extremes on average.

334

335 **3. Joint Distribution of Surface Temperature and SPEI:**

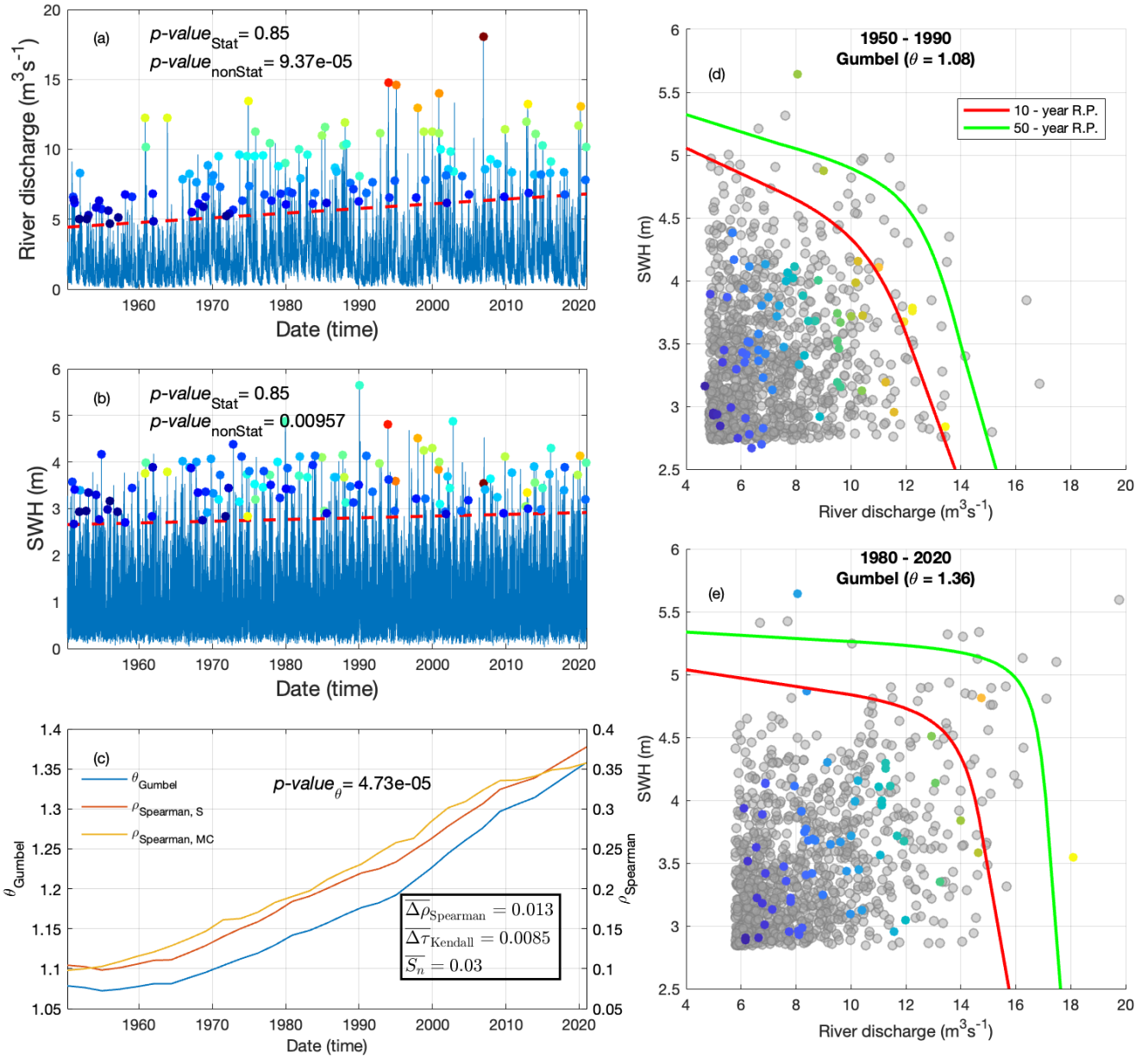
336 The third case study examined the relationship between surface temperature and the 6-month
337 Standardized Precipitation-Evapotranspiration Index (SPEI) in a region south of Milan, Italy (9.25E,
338 45.25N). Hourly surface temperature data from the ECMWF ERA-5 dataset (1959–2023) was paired
339 with monthly SPEI data (1959–2022) (Zhang, 2023). To better capture heatwave dynamics, the
340 temperature data were smoothed using a 10-day running mean. The analysis was restricted to the period
341 from April to September, which aligns with the growing season when drought impacts are at their peak
342 and heatwaves present a significant hazard. This case study demonstrated a scenario where block-
343 maxima sampling is a valid and simpler alternative to the POT method for analyzing extremes. A 35-
344 year non-stationary time window was used in this analysis for the joint distribution.
345
346

347 **3. Results**

348 **3.1. Case study 1: joint extremes of river discharge and wave height**

349 The non-stationarity of both time series was assessed using the Mann-Kendall test, which revealed
350 significant increasing trends in both variables (Fig. 2a–b). The effectiveness of transformation was
351 verified by p-values both before and after transformation (Fig. 2a-b). Among the evaluated copula
352 models, the Gumbel copula was the best fit for representing the dependence structure with this copula's
353 goodness of fit parameters presented in Fig. 2c. Applying a time-varying Gumbel copula with a 40-
354 year moving window revealed a statistically significant increasing trend in the dependency parameter,
355 denoted as θ_{Gumbel} (Fig. 1c). A similar upward trend was observed in the Spearman correlation
356 coefficient ρ_{Spearman} , calculated for both the sampled joint extremes and Monte Carlo-generated
357 samples.

358 To illustrate these findings, two representative time windows were selected, comparing the theoretical
359 Gumbel copula (gray dots, based on Monte Carlo simulations) with the sampled joint extremes (Fig.
360 2d–e). These panels visually confirmed a stronger coupling between the two variables toward the end
361 of the time series. This increase of coupling was also evident in shape of level curves corresponding to
362 10 and 50-year return periods. Furthermore, the analysis of joint return periods revealed substantial
363 shifts in level curves between the beginning and end of the series (curves in Fig. 2d–e), demonstrating
364 the utility of this technique in capturing temporal variations (non-stationarity) in joint extremes.
365



366
 367
 368
 369
 370
 371
 372
 373
 374
 375
 376

Figure 2: Analysis of joint extremes of river discharge and wave height off La Liane river mouth. In panels (a)-(b) the input series are presented (blue line). The thick dashed red line is the time-varying threshold level while the colored dots indicate the joint extreme events. The color of dots was based on events having the largest mean value. Also shown in these two plots is the p-value of Mann-Kendall test of the percentile series applied on both stationary (denoted by Stat) and non-stationary (denoted by nonStat) series. Variation with time of the copula parameter was depicted in panel (c) with a p-value of Mann-Kendall test. Other goodness-of-fit parameters of the non-stationary copula model were shown in panel (c). A 10-window smoothing was applied to curves of panel (c) for better representation. The time-varying Spearman correlation coefficient of the samples (red line) and Monte-Carlo values (yellow line) were also presented in panel (c). Panels (d) – (e) present the overlay of joint extremes (colored dots) and Monte-Carlo values (gray dots) in two different time windows (1950 – 1990) of (1980 – 2020) with the copula parameter indicated above. The 10 and 50-year joint return levels (using the AND definition) are also shown in these panels (colored curves).

377 3.2. Case study 2: trivariate joint extremes of significant wave height

378 The co-occurrence of extreme SWH at three locations (P1–P3) around the Marshall Islands was
379 examined as the second case study (Fig. 3). Univariate non-stationarity was evaluated using the Mann-
380 Kendall test (Fig. 3b, f, i), which revealed the strongest non-stationarity at P2, as indicated by its lowest
381 p-value. Both P1 and P3 also exhibited positive trends, significant at the 90% confidence level. The
382 effectiveness of transformation for each bivariate pair was assessed by comparing p-values before and
383 after transformation (Fig. 3b, f, i). The transformation clearly influenced the detected trends with all
384 pairs showing p-values greater than 0.7 after the stationarizing step.

385 Non-stationarity in the coupling was evaluated using a time-varying Gumbel copula model, showing
386 significant increasing trends in correlation for all pairs (p-value < 0.05) (Fig. 3e). Notably, the
387 correlations for P1–P3 and P1–P2 have p-values near zero, whereas the correlation for P2–P3 is
388 approximately 0.03 (Fig. 3e). The pairs of extremes of SWH exhibited a change in correlation with
389 time, with the Gumbel coupling parameter changing from 1.98 to 2.46 for P1–P2 pair, 2.05 to 2.43 in
390 P1–P3, and 1.42 to 1.61 in P2–P3 (Fig. 3c–d, g–h, j–k). The Monte Carlo extractions (gray dots in Fig.
391 3c–d, g–h, j–k) closely matched the data samples, demonstrating good agreement. The goodness-of-fit
392 metrics indicated accurate results, with $\overline{\Delta\rho_{Spearman}} = 0.13$, $\overline{\Delta\tau_{Kendall}} = 0.11$, $\overline{S_n} = 0.07$ (Fig. 3a).

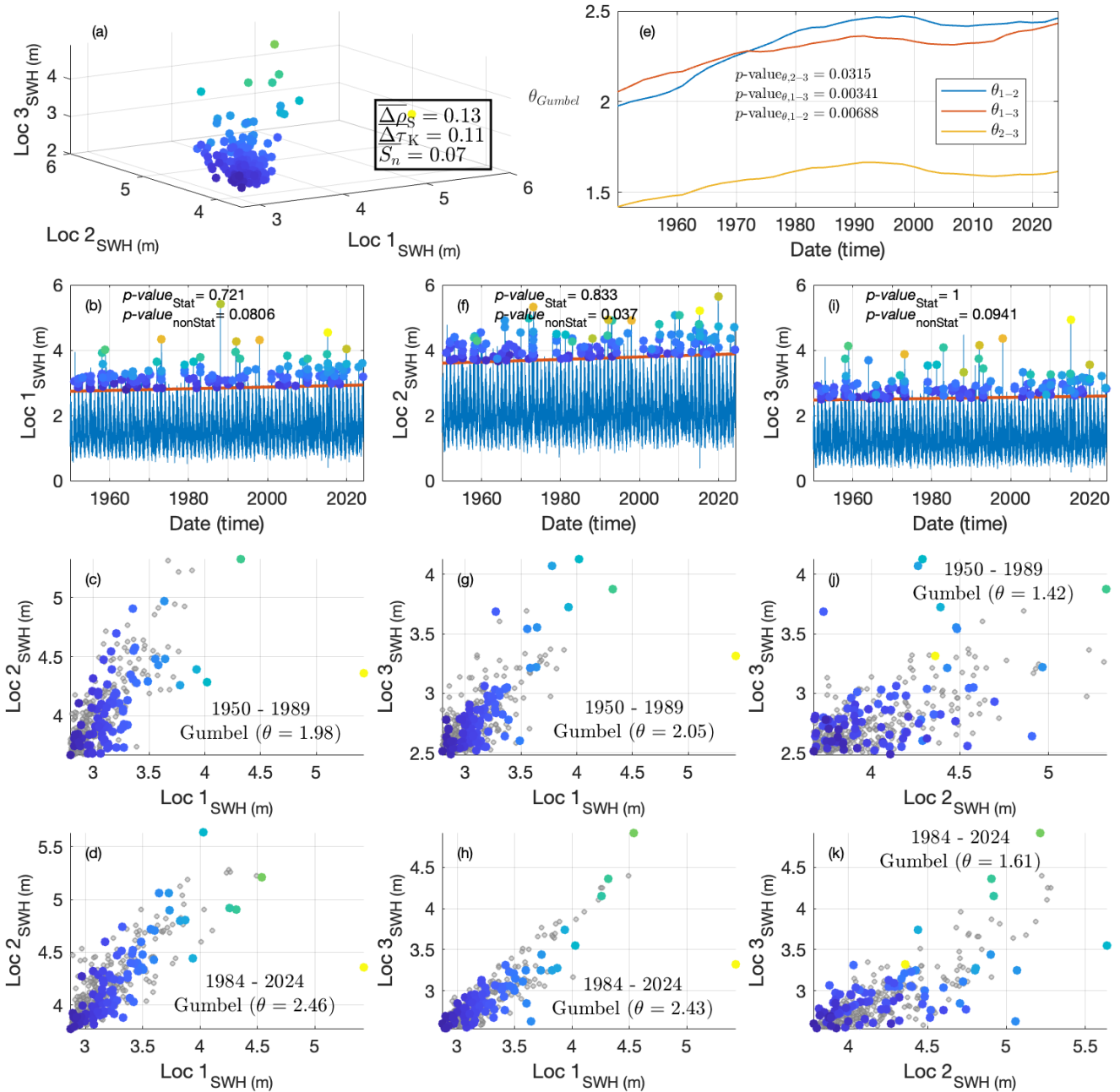
393

394

395

396

397



398
399
400
401
402
403
404
405

Figure 3: Analysis of trivariate extremes of SWH in neighboring locations near Marshall Islands. Goodness-of-fit parameters and sampled extremes are presented in panel (a). Univariate extremes (colored dots) and threshold levels (thick red lines) along with the p-value of the Mann-Kendall test of the percentile series applied on both stationary (denoted by Stat) and non-stationary (denoted by nonStat) series are presented in panels (b), (f) and (i). Panels (c), (d), (g), (j), (k) and (i) present overlaying of pairs of extremes (colored dots) and Monte-Carlo values (gray dots) with the copula parameter and time window indicated above each panel. The time-varying coupling parameter of each pair of extremes and the p-value of the Mann-Kendall test of the coupling parameter is presented in panel (e). A 10-window smoothing was applied to curves of panel (e).

406
407
408
409
410

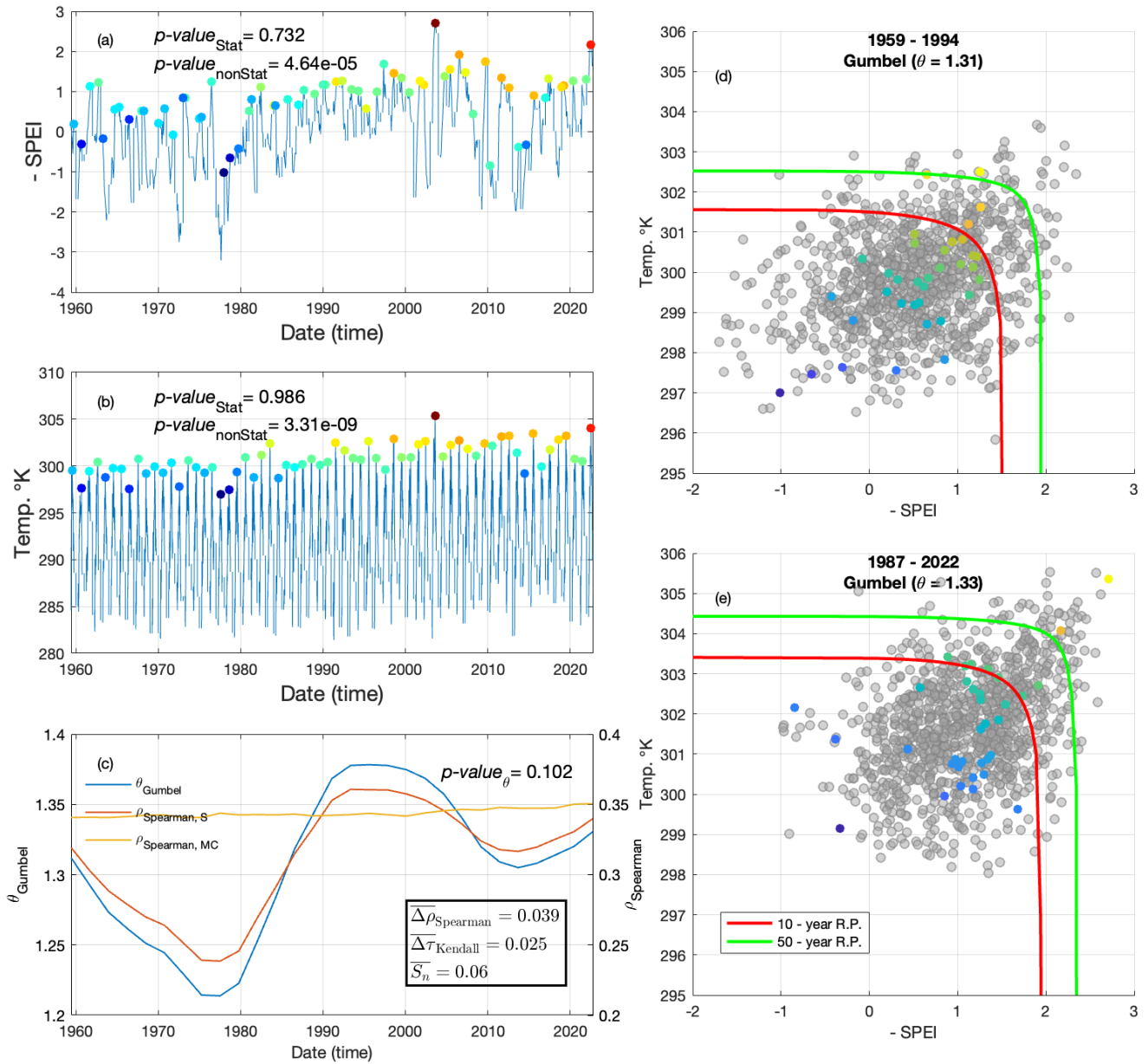
3.3. Case study 3: joint extremes of surface temperature and SPEI

The final case study examines joint extremes of surface temperature and the SPEI at an inland location south of Milan, focusing on the period from April to September. In this case, an annual maxima sampling technique was employed to identify univariate extremes (Fig. 4a–b), and the Gumbel copula

411 was used to model their joint distribution. Consequently, the marginals were estimated using the GEV
412 distribution.

413 Non-stationarity in both series was assessed through the Mann-Kendall test, with p-values close to zero
414 (Fig. 4a-b). The p-values increased significantly after the transformation based on comparison of p-
415 values obtained from original non-stationary and transformed stationary series (Fig. 4a-b). Based on
416 goodness-of-fit statistics ($\overline{\Delta\rho_{Spearman}}$, $\overline{\Delta\tau_{Kendall}}$ and $\overline{S_n}$), the Gumbel copula was identified as the best-
417 performing model for representing the joint distribution of extremes (Fig. 4c). The application of a non-
418 stationary Gumbel copula allowed for the estimation of a time-varying coupling parameter (blue curve
419 in Fig. 4c). However, unlike the previous two examples, no significant trend was detected in the time-
420 varying coupling parameter (Fig. 4c). This indicates that the non-stationarity in the joint distribution
421 was solely driven by the non-stationarity of the marginals. The Spearman correlation parameter of the
422 joint extremes also indicated lack of significant trend (red line; Fig. 4c). Thus, in this example a
423 constant coupling parameter was adopted (mean of the blue curve in Fig. 4c). Subsequently, the Monte-
424 Carlo samples generated based on the coupling parameter indicated near-constant Spearman correlation
425 parameter (yellow line; Fig. 4c). The evolving interrelationships of extremes was also verified by a
426 visual inspection of different time windows across the duration of series (Fig. 4d-e). Evidently, the
427 Gumbel copula was a good representation for co-occurrences of extremes, where stronger
428 dependencies was observed in the upper tail of both time windows (Fig. 4d-f). The non-stationarity of
429 the marginals resulted in change of level curves corresponding with 10 and 50-year joint return periods
430 (colored curves in Fig. 4d-f).

431



432
 433 *Figure 4: Analysis of annual extremes of SPEI and temperature (°C). Panels (a)–(b) display the input series (thin blue line) alongside the*
 434 *annual maxima (colored dots), where SPEI values have been multiplied by -1 for interpretability. The color of the dots reflects the mean*
 435 *values of the joint extremes. The p-value from the Mann-Kendall test applied on both stationary (denoted by Stat) and non-stationary*
 436 *(denoted by nonStat) series for the annual maxima is also reported in these panels. Panel (c) presents the goodness-of-fit parameters for*
 437 *the copula model, along with the time-varying coupling parameter (left axis) (thick blue line) and the time-varying Spearman*
 438 *correlation coefficient, calculated for both the original samples and the Monte Carlo values (right axis). A 10-window smoothing was applied to*
 439 *curves of panel (c) for better representation. Panels (d)–(e) overlay the joint extremes (colored dots) with Monte Carlo values (gray dots),*
 440 *simulated based on the constant coupling parameter specified in each panel. The level of agreement between the observed and simulated*
 441 *values demonstrates the validity of the fitted copula model. Also shown in these two panels is the joint return levels (using AND*
 442 *definition) corresponding with the 10 and 50-year return levels (colored curves).*

443 Discussion

444 Extreme Value Analysis (EVA) is a robust and widely used method for estimating the frequency of rare
 445 and impactful events. However, the growing availability of long-term, large-scale time series for

446 hazard-related variables, from both historical and climate studies, has increasingly demonstrated that
447 the assumption of stationarity, a cornerstone of EVA, often does not hold. In the case studies examined
448 in this research, statistically significant trends were observed across all the time series analyzed.
449 Moreover, beyond significant temporal changes in the extremes of many univariate series, clear non-
450 stationarity was also observed in the dependencies between different variables. This study highlights
451 the importance of considering non-stationarity in modeling joint distribution of natural hazard data.
452

453 The first case study explores the relationship between river discharge and coastal hazard-related
454 variables, such as significant wave height (SWH). While the coupling between these variables is
455 relatively weak, it remains statistically significant, indicating that the likelihood of compound events is
456 higher than would be expected if the variables were independent. Among the three tested copula
457 models, the Gumbel copula demonstrated the best fit, capturing the stronger dependency observed in
458 the upper tails. The analysis of the Liane River discharge and the SWH near its mouth over the past 70
459 years reveals a significant upward trend in both variables, as evidenced by p-values approaching zero
460 (Fig. 2a-b). Correspondingly, the coupling parameter has shown a marked increase over time, with the
461 Spearman correlation rising from less than 0.1 in 1950 (a low but statistically significant value) to over
462 0.37 in 2020 (Fig. 2c). This growing interdependence has led to a pronounced upward shift in the AND
463 return level curves (Fig. 2d-e). This significant growth in coupling may be attributed to two factors: the
464 inherent stronger upper-tail dependency captured by the Gumbel copula and the increasing frequency
465 of extreme values in both river discharge and SWH. These findings suggest that while the underlying
466 dynamics of the coupling have remained stable, the amplification of extremes in both variables have
467 intensified their overall interdependence during joint peak events.
468

469 The second case study investigates the spatial dependency of extremes in a hazard-related variable,
470 specifically significant wave height (SWH). This aspect is critical for risk assessment, as hazards often
471 exhibit strong spatial coherence. When an extreme event, such as a severe storm, impacts one location,
472 it is highly likely to affect neighboring areas as well. Consequently, hazards at different locations
473 cannot be assumed to be statistically independent (e.g., Vousdoukas et al., 2020). Previous studies have
474 examined spatial dependencies of extreme SWH using satellite altimeter observations or sparse buoy
475 data (e.g., Shooter et al., 2021; Jane et al., 2016; Wang et al., 2024). These works aimed to quantify
476 spatial dependence in extreme wave events, offering valuable insights for coastal inundation studies
477 and the creation of hazard maps. In this case study, high-resolution numerical wave model data from
478 Mentaschi et al. (2023) were employed to assess the spatial correlation of extreme SWH, accounting
479 for non-stationarity in the marginal distributions and coupling intensity. The analysis focused on three
480 locations near the Marshall Islands, approximately 250 km apart for P1-P2 and P1-P3, and 350 km
481 apart for P2-P3. These locations are in a region characterized by numerous small islands that act as
482 natural barriers, attenuating wave energy from certain directions. Despite these geographical features,
483 the dependency between the variables remains significant. The degree of coupling in extreme SWH
484 among the three locations shows a clear relationship with their spatial separation. The comparable
485 distances between P1-P2 and P1-P3 correspond to similar levels of dependency in extreme wave
486 events, with correlation values increasing from 1.98 and 2.05 at the start of the time series to 2.46 and
487 2.43 by its end, respectively. In contrast, the greater distance between P2-P3 results in a weaker
488 dependency, with correlations starting at about 1.42 and rising to 1.61 over the same period. The
489 growing dependency among SWH at the three locations is supported by the Mann-Kendall test applied
490 to the coupling parameter. The test results indicate a p-value near zero for the pairs P1-P2 and P1-P3,
491 while the pair P2-P3 has a p-value of approximately 0.03. This observed increase in spatial dependency
492 across all pairs suggests that not only have extreme events intensified in the region, but their spatial
493 extent may have also expanded, affecting larger areas over time.

494

495 The third case study focuses on two hazard-related variables, temperature (a proxy for heatwaves) and
496 the SPEI, a proxy of drought, in the Milan area of Italy, both of which are strongly influenced by non-
497 stationarity. The coupling between these variables is well-documented, arising from the interplay
498 between temperature-driven evapotranspiration and the development of dry conditions. At the same
499 time, dry conditions lead to reduced evapotranspiration and greater heat accumulation on land surfaces
500 (e.g., Manning et al., 2019). However, previous studies (e.g., Ribeiro et al., 2020) have often
501 overlooked the impacts of non-stationarity when assessing the joint distribution of their extremes.
502 It is true that the asymptotic justification for the GEV distribution relies on block independence (or
503 weak dependence), and that slowly-varying seasonal phenomena such as droughts and heat waves
504 exhibit temporal correlation structures that may challenge these assumptions. Although SPEI-6
505 represents a slowly-developing process, the GEV distribution has been shown to provide adequate fits
506 for such variables at appropriate aggregation scales. Stagge et al. (2015) demonstrated that GEV
507 outperformed alternative distributions for SPEI across Europe for accumulation periods from 1 to 12
508 months. For the moderate temporal aggregations considered here (monthly temperature, SPEI-6), the
509 GEV provides a practical and empirically supported approximation for extreme value analysis.
510 Alternative approaches such as stochastic generation methods (Parey and Gailhard, 2022) may offer
511 additional rigor for specific applications with stronger temporal dependence. Our analysis revealed
512 pronounced non-stationarity in both variables, with p-values from the Mann-Kendall test close to zero
513 (Fig. 4a-b), clearly associated with ongoing climate change and global warming. The Gumbel copula
514 was found to be the most appropriate model for the joint distribution of SPEI and temperature,
515 highlighting their strong coupling during extreme events. Unlike the other two case studies, however,
516 the coupling between these variables lacked a significant trend. This was evidenced by the Mann-
517 Kendall test on the time-varying coupling parameter, which resulted in a p-value of 0.102 (Fig. 4c).
518 Given the low significance of the temporal change in the coupling between temperature and SPEI, this
519 case study presented an application where the joint behavior modelled by a Gumbel copula was mostly
520 influenced by non-stationarity of the marginals.

521

522 Final remarks

523

524 In this study, we extended the methodology for non-stationary Extreme Value Analysis (EVA)
525 proposed by Mentaschi et al. (2016) to enable the modeling of joint distributions of extremes that
526 evolve over time. This advancement addresses a critical limitation of univariate EVA, which cannot
527 account for the interdependence among extremes—a crucial aspect in accurately assessing hazards.
528 The framework was tested across a set of case studies involving different hazard-related variables, each
529 exhibiting varying degrees of non-stationarity and interdependence. These examples demonstrate the
530 versatility and generality of the methodology, to accommodate a wide range of environmental variables
531 with distinct characteristics in how extremes are sampled and evolve over the long term. Furthermore,
532 the framework includes techniques to evaluate the significance of modeled changes, enhancing its
533 utility for risk assessment.
534 A remarkable fact is that, in two out of the three case studies, not only do the univariate hazard-related
535 variables exhibit significant temporal changes, but their interdependence also evolves substantially over
536 time. This highlights the importance of adopting a methodology capable of addressing such dynamic
537 relationships, underscoring the relevance of the proposed approach.

538 Additionally, the framework incorporates built-in tools for Monte Carlo simulations, which are
539 instrumental in evaluating goodness-of-fit and estimating uncertainty. Beyond these applications, these
540 simulations can support a more comprehensive risk analysis by generating statistically consistent
541 hazard scenarios, further extending the utility of the methodology.
542 To support future research and applications, we have developed an open-source toolbox, tsEVA 2.0,
543 which accompanies this study. The toolbox, along with the data and examples presented in this paper,
544 is freely available online, offering a practical resource for exploring the joint distributions of non-
545 stationary extremes and fostering advancements in hazard and risk assessment.

548 Acknowledgements

549 This research has been supported by the European Space Agency (ESA) through the EOatSEE project,
550 contract n° 4000138378/22/I-DT, under the Earth Observation Science for Society block of activities,
551 part of the FutureEO-1 programme. We thank the reviewers for their feedback.

553 Code and data availability

554 The MATLAB toolbox presented in this paper is available at <https://doi.org/10.5281/zenodo.19087463>
555 and at the GitHub repository <https://github.com/menta78/tsEva>, together with the data and scripts used
556 to generate the figures. An interactive agentic assistant (Tessa M), designed to guide users through the
557 tsEVA 2.0 workflow, is available as a custom GPT at [https://chatgpt.com/g/g-
558 69a72fb764048191ae68e2201f7741a3-tessa-m](https://chatgpt.com/g/g-69a72fb764048191ae68e2201f7741a3-tessa-m) and as an agent embedded in the repository, accessible
559 via GitHub Copilot.

561 Author contributions

562 M.H. Bahmanpour: conceptualization, software development, data analysis, manuscript drafting. L.
563 Mentaschi: conceptualization, supervision, software development, manuscript drafting. G. Coppini:
564 results investigation, manuscript review, funding. Others: results investigation and manuscript review.

566 Competing interests

567 The authors declare that they have no competing interests.

569 REFERENCES

- 570
571 Acero, F. J., Parey, S., Hoang, T. T. H., Dacunha-Castelle, D., García, J. A., and Gallego, M. C.: Non-stationary future return
572 levels for extreme rainfall over Extremadura (southwestern Iberian Peninsula), *Hydrological Sciences Journal*, 62(9), 1394–
573 1411, <https://doi.org/10.1080/02626667.2017.1328559>, 2017.
- 574 Bevacqua, E., Maraun, D., Hobæk Haff, I., Widmann, M., and Vrac, M.: Multivariate statistical modelling of compound
575 events via pair-copula constructions: analysis of floods in Ravenna (Italy), *Hydrology and Earth System Sciences*, 21(6),
576 2701–2723, <https://doi.org/10.5194/hess-21-2701-2017>, 2017.
- 577 Bevacqua, E., Maraun, D., Vousdoukas, M. I., Voukouvalas, E., Vrac, M., Mentaschi, L., and Widmann, M.: Higher
578 probability of compound flooding from precipitation and storm surge in Europe under anthropogenic climate change, *Science
579 Advances*, 5(9), eaaw5531, <https://doi.org/10.1126/sciadv.aaw5531>, 2019.

580 Bender, J., Wahl, T., and Jensen, J.: Multivariate design in the presence of non-stationarity, *Journal of Hydrology*, 514, 123–
581 130, <https://doi.org/10.1016/j.jhydrol.2014.04.017>, 2014.

582 Cannon, A. J.: A flexible nonlinear modelling framework for nonstationary generalized extreme value analysis in
583 hydroclimatology, *Hydrological Processes*, 24(6), 673–685, <https://doi.org/10.1002/hyp.7506>, 2010.

584 Cheng, L., AghaKouchak, A., Gilleland, E., and Katz, R. W.: Non-stationary extreme value analysis in a changing climate,
585 *Climatic Change*, 127(2), 353–369, <https://doi.org/10.1007/s10584-014-1254-5>, 2014.

586 Coles, S.: *An introduction to statistical modeling of extreme values*, Springer, 2001.

587 Dosio, A., Mentaschi, L., Fischer, E. M., and Wyser, K.: Extreme heat waves under 1.5 °C and 2 °C global warming,
588 *Environmental Research Letters*, 13(5), 054006, <https://doi.org/10.1088/1748-9326/aab827>, 2018.

589 Dottori, F., Mentaschi, L., Bianchi, A., Alfieri, L., and Feyen, L.: Cost-effective adaptation strategies to rising river flood risk
590 in Europe, *Nature Climate Change*, 13(2), 196–202, <https://doi.org/10.1038/s41558-022-01540-0>, 2023.

591 Genest, C., Rémillard, B., and Beaudoin, D.: Goodness-of-fit tests for copulas: A review and a power study, *Insurance:
592 Mathematics and Economics*, 44(2), 199–213, <https://doi.org/10.1016/j.insmatheco.2007.10.005>, 2009.

593 Hamed, K. H.: Trend detection in hydrologic data: The Mann–Kendall trend test under the scaling hypothesis, *Journal of
594 Hydrology*, 349(3), 350–363, <https://doi.org/10.1016/j.jhydrol.2007.11.009>, 2008.

595 Hamed, K. H. and Rao, A. R.: A modified Mann-Kendall trend test for autocorrelated data, *Journal of Hydrology*, 204(1),
596 182–196, [https://doi.org/10.1016/S0022-1694\(97\)00125-X](https://doi.org/10.1016/S0022-1694(97)00125-X), 1998.

597 Jane, R., Dalla Valle, L., Simmonds, D., and Raby, A.: A copula-based approach for the estimation of wave height records
598 through spatial correlation, *Coastal Engineering*, 117, 1–18, <https://doi.org/10.1016/j.coastaleng.2016.06.008>, 2016.

599 Jiang, C., Xiong, L., Xu, C.-Y., and Guo, S.: Bivariate frequency analysis of nonstationary low-flow series based on the time-
600 varying copula, *Hydrological Processes*, 29(6), 1521–1534, <https://doi.org/10.1002/hyp.10288>, 2015.

601 Jiang, S., Bevacqua, E., and Zscheischler, J.: River flooding mechanisms and their changes in Europe revealed by explainable
602 machine learning, *Hydrology and Earth System Sciences*, 26(24), 6339–6359, <https://doi.org/10.5194/hess-26-6339-2022>,
603 2022.

604 Joe, H.: *Multivariate Models and Multivariate Dependence Concepts*, Chapman and Hall/CRC,
605 <https://doi.org/10.1201/9780367803896>, 1997.

606 Li, H., Wang, D., Singh, V. P., Wang, Y., Wu, J., Wu, J., Liu, J., Zou, Y., He, R., and Zhang, J.: Non-stationary frequency
607 analysis of annual extreme rainfall volume and intensity using Archimedean copulas: A case study in eastern China, *Journal
608 of Hydrology*, 571, 114–131, <https://doi.org/10.1016/j.jhydrol.2019.01.054>, 2019.

609 Manning, C., Widmann, M., Bevacqua, E., van Loon, A. F., Maraun, D., and Vrac, M.: Increased probability of compound
610 long-duration dry and hot events in Europe during summer (1950–2013), *Environmental Research Letters*, 14(9), 094006,
611 <https://doi.org/10.1088/1748-9326/ab23bf>, 2019.

612 Mentaschi, L., Vousdoukas, M. I., Voukouvalas, E., Sartini, L., Feyen, L., Besio, G., and Alfieri, L.: The transformed-
613 stationary approach: a generic and simplified methodology for non-stationary extreme value analysis, *Hydrology and Earth
614 System Sciences*, 20(9), 3527–3547, <https://doi.org/10.5194/hess-20-3527-2016>, 2016.

615 Mentaschi, L., Vousdoukas, M. I., Voukouvalas, E., Dosio, A., and Feyen, L.: Global changes of extreme coastal wave energy
616 fluxes triggered by intensified teleconnection patterns, *Geophysical Research Letters*, 44(5), 2416–2426,
617 <https://doi.org/10.1002/2016GL072488>, 2017.

618 Mentaschi, L., Vousdoukas, M. I., García-Sánchez, G., Fernández-Montblanc, T., Roland, A., Voukouvalas, E., Federico, I.,
619 Abdolali, A., Zhang, Y. J., and Feyen, L.: A global unstructured, coupled, high-resolution hindcast of waves and storm surge,
620 *Frontiers in Marine Science*, 10, <https://doi.org/10.3389/fmars.2023.1233679>, 2023.

621 Naumann, G., Cammalleri, C., Mentaschi, L., and Feyen, L.: Increased economic drought impacts in Europe with
622 anthropogenic warming, *Nature Climate Change*, 11(6), 485–491, <https://doi.org/10.1038/s41558-021-01044-3>, 2021.

623 Nelsen, R. B.: An introduction to copulas, Springer, <https://doi.org/10.1007/0-387-28678-0>, 2006.

624 Parey, S., Hoang, T. T. H., and Dacunha-Castelle, D.: Different ways to compute temperature return levels in the climate
625 change context, *Environmetrics*, 21(7–8), 698–718, <https://doi.org/10.1002/env.1060>, 2010.

626 Parey, S., Hoang, T. T. H., and Dacunha-Castelle, D.: The importance of mean and variance in predicting changes in
627 temperature extremes, *Journal of Geophysical Research: Atmospheres*, 118(15), 8285–8296,
628 <https://doi.org/10.1002/jgrd.50629>, 2013.

629 Parey, S., Hoang, T. T. H., and Dacunha-Castelle, D.: Future high-temperature extremes and stationarity, *Natural Hazards*,
630 98(3), 1115–1134, <https://doi.org/10.1007/s11069-018-3499-1>, 2019.

631 Parey, S. and Gailhard, J.: Extreme Low Flow Estimation under Climate Change, *Atmosphere*, 13(2),
632 <https://doi.org/10.3390/atmos13020164>, 2022.

633 Ribeiro, A. F. S., Russo, A., Gouveia, C. M., and Pires, C. A. L.: Drought-related hot summers: A joint probability analysis
634 in the Iberian Peninsula, *Weather and Climate Extremes*, 30, 100279, <https://doi.org/10.1016/j.wace.2020.100279>, 2020.

635 Salvadori, G., Durante, F., de Michele, C., Bernardi, M., and Petrella, L.: A multivariate copula-based framework for dealing
636 with hazard scenarios and failure probabilities, *Water Resources Research*, 52(5), 3701–3721,
637 <https://doi.org/10.1002/2015WR017225>, 2016.

638 Sarhadi, A., Burn, D. H., Concepción Ausín, M., and Wiper, M. P.: Time-varying nonstationary multivariate risk analysis
639 using a dynamic Bayesian copula, *Water Resources Research*, 52(3), 2327–2349, <https://doi.org/10.1002/2015WR018525>,
640 2016.

641 Seinaldi, F.: Dismissing return periods!, *Stochastic Environmental Research and Risk Assessment*, 29(4), 1179–1189,
642 <https://doi.org/10.1007/s00477-014-0916-1>, 2015.

643 Shooter, R., Ross, E., Ribal, A., Young, I. R., and Jonathan, P.: Spatial dependence of extreme seas in the North East Atlantic
644 from satellite altimeter measurements, *Environmetrics*, 32(4), e2674, <https://doi.org/10.1002/env.2674>, 2021.

645 Sklar, A.: Fonctions de répartition à n dimensions et leurs marges, *Publications de l’Institut de Statistique de l’Université de*
646 *Paris*, 8, 229–231, 1959.

647 Sklar, A.: Random variables, joint distribution functions, and copulas, *Kybernetika*, 9(6), 449–460, 1973.

648 Stagge, J. H., Tallaksen, L. M., Gudmundsson, L., van Loon, A. F., and Stahl, K.: Candidate distributions for climatological
649 drought indices (SPI and SPEI), *International Journal of Climatology*, 35(13), 4027–4040, <https://doi.org/10.1002/joc.4267>,
650 2015.

651 Tilloy, A., Malamud, B. D., Winter, H., and Joly-Laugel, A.: Evaluating the efficacy of bivariate extreme modelling
652 approaches for multi-hazard scenarios, *Natural Hazards and Earth System Sciences*, 20(8), 2091–2117,
653 <https://doi.org/10.5194/nhess-20-2091-2020>, 2020.

654 Tilloy, A., Paprotny, D., Grimaldi, S., Gomes, G., Bianchi, A., Lange, S., Beck, H., Mazzetti, C., and Feyen, L.: HERA: a
655 high-resolution pan-European hydrological reanalysis (1951–2020), *Earth System Science Data*, 17(1), 293–316,
656 <https://doi.org/10.5194/essd-17-293-2025>, 2025.

657 Wahl, T., Jain, S., Bender, J., Meyers, S. D., and Luther, M. E.: Increasing risk of compound flooding from storm surge and
658 rainfall for major US cities, *Nature Climate Change*, 5(12), 1093–1097, <https://doi.org/10.1038/nclimate2736>, 2015.

659 Wang, R., Liu, J., and Wang, J.: The extremal spatial dependence of significant wave height in the South China sea, *Ocean
660 Engineering*, 295, 116888, <https://doi.org/10.1016/j.oceaneng.2024.116888>, 2024.

661 Vousdoukas, M. I., Mentaschi, L., Voukouvalas, E., Verlaan, M., Jevrejeva, S., Jackson, L. P., and Feyen, L.: Global
662 probabilistic projections of extreme sea levels show intensification of coastal flood hazard, *Nature Communications*, 9(1),
663 2360, <https://doi.org/10.1038/s41467-018-04692-w>, 2018.

664 Vousdoukas, M. I., Mentaschi, L., Hinkel, J., Ward, P. J., Mongelli, I., Ciscar, J.-C., and Feyen, L.: Economic motivation for
665 raising coastal flood defenses in Europe, *Nature Communications*, 11(1), 2119, <https://doi.org/10.1038/s41467-020-15665-3>,
666 2020.

667 Yue, S. and Wang, C.: The Mann-Kendall test modified by effective sample size to detect trend in serially correlated
668 hydrological series, *Water Resources Management*, 18(3), 201–218,
669 <https://doi.org/10.1023/B:WARM.0000043140.61082.60>, 2004.

670 Zscheischler, J., Martius, O., Westra, S., Bevacqua, E., Raymond, C., Horton, R. M., van den Hurk, B., AghaKouchak, A.,
671 Jézéquel, A., Mahecha, M. D., Maraun, D., Ramos, A. M., Ridder, N. N., Thiery, W., and Vignotto, E.: A typology of
672 compound weather and climate events, *Nature Reviews Earth & Environment*, 1(7), 333–347, <https://doi.org/10.1038/s43017-020-0060-z>, 2020.

674 Zscheischler, J., Westra, S., van den Hurk, B. J. J. M., Seneviratne, S. I., Ward, P. J., Pitman, A., AghaKouchak, A., Bresch,
675 D. N., Leonard, M., Wahl, T., and Zhang, X.: Future climate risk from compound events, *Nature Climate Change*, 8(6), 469–
676 477, <https://doi.org/10.1038/s41558-018-0156-3>, 2018.

677 Zheng, F., Westra, S., Leonard, M., and Sisson, S. A.: Modeling dependence between extreme rainfall and storm surge to
678 estimate coastal flooding risk, *Water Resources Research*, 50(3), 2050–2071, <https://doi.org/10.1002/2013WR014616>, 2014.

679 Zhang, X.: A dataset of monthly SPI and SPEI derived from ERA5 over 1959–2022, Figshare [data set],
680 <https://doi.org/10.6084/m9.figshare.24485389.v1>, 2023.